DALTON
FULL PAPER

Spectroscopic characterisation of electrogenerated nickel(III) species. Complexes with N_2O_2 Schiff-base ligands derived from salicylaldehyde

Cristina Freire and Baltazar de Castro *

CEQUP/Departamento de Química, Faculdade de Ciências, Universidade do Porto, 4150 Porto, Portugal

Several nickel(II) complexes with tetradentate N_2O_2 Schiff-base ligands (H_2L) have been synthesized and their oxidative chemistry studied in dimethylformamide and in dimethyl sulfoxide. Electrochemical and EPR data for the oxidised solution revealed that in these strong co-ordinated solvents almost all nickel(II) complexes were oxidised to low-spin six-co-ordinate nickel(III) complexes, formulated as $[Ni^{III}L(solv)_2]^+$, where solv stands for a solvent molecule. Upon addition of pyridine to fluid solutions of $[Ni^{III}L(solv)_2]^+$ new species were formed which on the basis of their EPR spectra can be formulated as $[Ni^{III}L(py)_2]^+$. Extensive electronic characterisation of the nickel(III) compounds was made by coupling of EPR and electronic spectroscopic data.

High-valence nickel chemistry has attracted increased attention as it has become clear that the +3 oxidation state is biologically significant.[1] More recently, it was found that high-valent nickel species may also be intermediates in newly discovered catalytic oxidations,[2] and in the nickel-mediated sequence-specific oxidative cleavage of DNA by designed metalloproteins.[3]

There is a considerable interest in knowledge of the factors that modulate oxidative behaviour of nickel(II) complexes with macrocyclic [1a,4–7] and other polydentate ligands,[1a,8–12] and in the characterisation of their electronic structure in order to understand the role of natural occurring and synthetic nickel(III) complexes in their catalytic cycles. Moreover, this information will be useful in the design of new complexes with well defined catalytic properties.

We have been interested in the study of nickel-(I) and -(III) complexes with Schiff-base ligands having mixed co-ordination spheres.[10–15] Identification of the factors that control the oxidation/reduction site in these complexes, determination of their redox potentials and characterisation of their electronic structure have been the main purposes of the ongoing work. These complexes afford two main differences relative to macrocyclic ligands: easier access to mixed-donor environments, and an open equatorial ring the hole size of which can in principle accommodate more easily the expected changes in metal size upon oxidation/reduction.

Nickel(II) complexes with tetradentate N_2O_2 Schiff-base ligands derived from salicylaldehyde have been known for a long time.[16] Nevertheless their redox properties are currently a theme of interest since these complexes provide examples of systems where the final reduction/oxidation site (metal or ligand) can be controlled by the aromaticity of the ligand (reduction process) [12,17] and by the solvent (oxidation process).[10,11,18,19]

Our interest in the chemistry and reactivity of high-valent nickel complexes has led us to perform a systematic investigation on the oxidative chemistry of nickel(II) complexes with tetradentate N_2O_2 Schiff-base ligands formed by condensation of salicylaldehyde derivatives with several diamines (Scheme 1). We have shown [10–12] that in strong donating solvents such complexes are oxidised to nickel(III) species; however in acetonitrile and in other lower co-ordinating solvents they are oxidatively polymerised at the electrode surfaces to generate electroactive films the physical/chemical properties of which have been a matter of controversy.[19–21] Recently, we have reinvestigated the oxidation of [Ni(salen)] in acetonitrile [22] and by coupling spectroscopic (FTIR, UV/VIS and EPR) and electrochemical

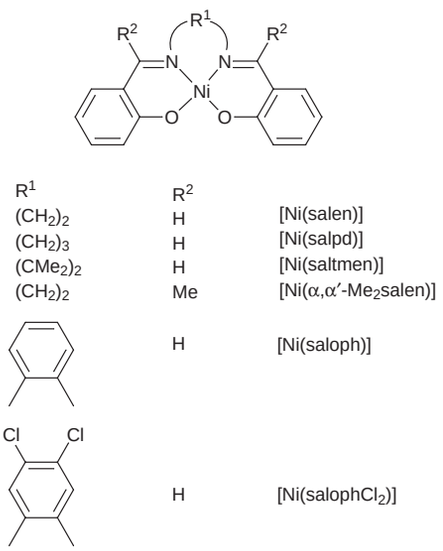

Scheme 1

techniques have demonstrated that polymerisation is ultimately a ligand-based process and the resulting polymer exhibits physical/chemical properties that cannot be attributed to an aggregation of individual nickel-(II) or -(III) complexes, behaving rather like a polyphenylene compound.

We have extended this study, in order to get insights into the relative influence of the equatorial/axial ligand field in stabilising the +3 oxidation state of the metal. Hence, the electrochemical properties of the complexes in Scheme 1 were studied in dimethylformamide and dimethyl sulfoxide, using NEt_4ClO_4 as supporting electrolyte. The complexes were oxidised by controlled-potential electrolysis in these solvents and their pyridine adducts were also prepared. Extensive electronic characterisation of the nickel(III) species was obtained by coupling EPR and electronic spectroscopic data.

Experimental

Reagents, solvents, and ligands

The solvents for syntheses were of reagent grade and those for electrochemical measurements were of analytical grade; all were used as received. All reagents (nickel acetate tetrahydrate, salicylaldehyde, *o*-phenylenediamine, ethane-1,2-diamine, 2-

hydroxyacetophenone, 4,5-dichloro-1,2-phenylenediamine, 1,3-diaminopropane, 2,3-dimethyl-2,3-dinitrobutane, tetraethylammonium bromide and perchloric acid) were obtained commercially and used as received, except for ethane-1,2-diamine which was distilled prior to use. 2-3-Dimethylbutane-2,3-diamine was prepared by a modification of the method of Sayre.[23] Tetraethylammonium perchlorate was prepared by published procedures from tetraethylammonium bromide and perchloric acid.[24] **CAUTION**: perchlorates are hazardous and may explode.

The Schiff bases were prepared by standard methods,[16,25] in which an ethanolic solution of a diamine was added to a rapidly stirred ethanolic solution of salicylaldehyde and the resulting mixture was then refluxed. On cooling to room temperature, the yellow solids formed were filtered off, washed with cold ethanol and cold diethyl ether, and dried under vacuum for several hours.

Nickel complexes

Nickel(II) complexes were also synthesized by standard procedures:[16] ethanolic solutions of the Schiff base were added to ethanolic nickel(II) acetate solutions and the resulting mixtures refluxed; after cooling, brown or red-brown microcrystalline solids were filtered off, washed with ethanol and diethyl ether, and dried under vacuum. Several of these complexes have been studied previously; their inclusion provides a complete and coherent framework for the overall study reported here.

[Ni(salen)]: ^{1}H NMR ($CDCl_3$, 200 MHz, 297 K): δ 3.44 (4 H, CH_2CH_2), 6.52–7.19 (8 H, aromatic H) and 7.41 (2 H, =CH). Electronic spectra: λ_{max}/nm(ε/dm^3 mol^{-1} cm^{-1}) 540 (230), 440 (3860), 405 (7170) and 390 (4560) (Me_2SO); 540, 430, 410 and 370 (Nujol) (Found: C, 59.2; H, 4.3; N, 8.6. Calc. for $C_{16}H_{14}N_2NiO_2$: C, 59.1; H, 4.3; N, 8.6%).

[Ni(saltmen)]: ^{1}H NMR ($CDCl_3$, 200 MHz, 297 K): δ 1.44 [12 H, $C(CH_3)_2C(CH_3)_2$], 6.48–7.26 (8 H, aromatic H) and 7.48 (2 H, =CH). Electronic spectra: λ_{max}/nm(ε/dm^3 mol^{-1} cm^{-1}) 545 (160), 435 (4000), 410 (7000) and 390 (4250) (Me_2SO); 545, 440, 410 and 390 (Nujol) (Found: C, 62.9; H, 5.9; N, 7.4. Calc. for $C_{20}H_{24}N_2NiO_2$: C, 63.0; H, 5.8; N, 7.4%).

[Ni(α,α′-Me_2salen)]: ^{1}H NMR [$(CD_3)_2SO$, 200 MHz, 297 K]: δ 2.35 [6 H, $=C(CH_3)$] 3.43 (4 H, CH_2CH_2) and 6.43–7.52 (8 H, aromatic H). Electronic spectra: λ_{max}/nm(ε/dm^3 mol^{-1} cm^{-1}) 545 (160), 445 (2600), 405 (6170) and 390 (4670) (Me_2SO); 545, 445, 415 and 390 (Nujol) (Found: C, 59.9; H, 5.2; N, 7.7. Calc. for $C_{18}H_{20}N_2NiO_2\cdot0.5H_2O$: C, 59.7; H, 5.3; N, 7.7%).

[Ni(salpd)]: ^{1}H NMR (low solubility in the solvents used). Electronic spectra: λ_{max}/nm(ε/dm^3 mol^{-1} cm^{-1}) 500, 410, 375 and 355 (Me_2SO); 590 (Nujol) (Found: C, 59.5; H, 4.4; N, 7.9. Calc. for $C_{17}H_{16}N_2NiO_2$: C, 60.2; H, 4.7; N, 8.2%).

[Ni(saloph)]: ^{1}H NMR ($CDCl_3$, 200 MHz, 297 K): δ 6.62–7.75 (12 H, aromatic H) and 8.25 (2 H, =CH). Electronic spectra: λ_{max}/nm(ε/dm^3 mol^{-1} cm^{-1}) 475 (9300), 450 (8000), 375 (28 000) and 365 (24 000) (Me_2SO); 570, 520, 490, 450 and 390 (Nujol) (Found: C, 64.3; H, 3.7; N, 7.4. Calc. for $C_{20}H_{14}N_2NiO_2$: C, 64.4; H, 3.8; N, 7.5%).

[Ni(salophCl$_2$)]: ^{1}H NMR [$(CD_3)_2SO$, 200 MHz, 297 K]: δ 6.63–8.45 (10 H, aromatic H) and 9.00 (2 H, =CH). Electronic spectra: λ_{max}/nm(ε/dm^3 mol^{-1} cm^{-1}) 490 (10 500), 455 (8850), 383 (29 800) and 360 (21 200) (Me_2SO); 560, 535, 500, 450 and 400 (Nujol) (Found: C, 54.0; H, 2.7; N, 6.2. Calc. for $C_{20}H_{14}Cl_2N_2NiO_2$: C, 54.4; H, 2.7; N, 6.3%).

Preparations of nickel(III) complexes were attempted by electrochemical oxidation of solutions 1 mmol dm^{-3} in the corresponding nickel(II) complexes with NEt_4ClO_4 (0.1 mol dm^{-3}) as support electrolyte, in the following solvents: (a) dmf at −20 °C and (b) Me_2SO at room temperature. Owing to instability of the electrogenerated nickel(III) species it was not possible to isolate solids; the electrogenerated species were prepared shortly before measurements and kept frozen in liquid nitrogen. Manipulations of nickel(III) species were carried out in a nitrogen atmosphere, by use of standard Schlenk techniques and/or of a glove-box.

Pyridine adducts were prepared by addition of cold solutions of pyridine in toluene (10 fold-in excess of metal complexes) to freshly electrolysed solutions of Ni^{III} that had been frozen and then warmed to just above the softening point of the frozen glass. The resulting solutions were immediately transferred to EPR tubes and then frozen in liquid nitrogen.

Physical measurements

Elemental analyses (C, H and N) were performed at the Microanalytical Laboratory, University of Manchester. Proton NMR spectra were recorded with a Bruker AC 200 spectrometer at 25 °C, using $SiMe_4$ as internal reference.

Electrochemical measurements were made with a E 611 VA-Detector, a E 612 VA-Scanner, and a E 524 coulometer (all from Metrohm) using dmf or Me_2SO solutions 1 mmol dm^{-3} in nickel(II) complex and 0.1 mol dm^{-3} NEt_4ClO_4. Cyclic voltammetry was performed using a platinum microsphere as working electrode, a platinum wire as counter electrode, and an Ag–AgCl (1 mol dm^{-3} NaCl) reference electrode. All potentials are reported relative to that of the reference electrode and to $E_{\frac{1}{2}}$ of the ferrocenium–ferrocene couple; under the experimental conditions used (scan rate 0.05 V s^{-1}) $E_{\frac{1}{2}}$ for latter couple is 0.50 V in dmf ($\Delta E = 0.10$ V) and 0.48 V in Me_2SO ($\Delta E = 0.09$ V). Measured potentials were not corrected for liquid-junction potentials. Scan rates from 0.01 to 0.10 V s^{-1} were used and the low and high potential limits were 0.30 and 1.30 V.

Electrolyses were carried out at controlled potential at a value 0.05 V higher than the anodic peak potential in a three-electrode cell, using a platinum gauze as working electrode, a platinum foil as counter electrode, and an Ag–AgCl (1 mol dm^{-3} NaCl) reference electrode.

The EPR spectra were obtained with an X-band Varian E 109 spectrometer at 77 K. Spectra were calibrated with diphenylpicrylhydrazyl (dpph; $g = 2.0037$) and the magnetic field was calibrated by use of Mn^{2+} in MgO. The reported EPR parameters were obtained by computer simulation.[26] Nickel(III) concentrations were estimated by double integration of EPR spectra, including baseline and Aasa and Vänngard corrections,[27] using Me_2SO solutions of copper(II) nitrate as concentration standards.

Room-temperature electronic spectra of nickel(II,III) complexes in solutions of dmf and Me_2SO and of nickel(II) complexes in Nujol mulls were recorded with a Cary 17DX spectrophotometer. Molar absorption coefficients for the nickel(III) electronic bands were estimated by using the values of the nickel(III) concentration obtained from EPR spectra.

Results and Discussion

Structural and electronic data for nickel(II) complexes

Crystal and molecular structures are known for [Ni(salen)],[28] [Ni(salpd)],[29] [Ni(α,α′-Me_2salen)],[30] [Ni(saloph)],[31] and the co-ordination geometry around the metal atom has been found to be square planar in all the complexes, with the ligand co-ordinated through the nitrogen and oxygen atoms in a N_2O_2 *cis* configuration. The N_2O_2 co-ordination sphere is almost planar with the metal atom lying practically in the plane defined by the co-ordinated atoms, except in [Ni(salpd)] for which the nickel atom is 12 pm out of this plane.[29] The aromatic imine bridges are necessarily planar, whereas aliphatic bridges are normally puckered with several atoms deviating from the best co-ordination plane. As a consequence, in complexes with aromatic bridges the Ni–N bond distances are longer than Ni–O, a situation that is reversed in complexes with aliphatic bridges.

The similarity between the electronic data for the above complexes and for those for which no crystal data are available is taken to provide support to the assumption that all complexes

Table 1 Cyclic voltammetric results for nickel(II) complexes in dmf and Me_2SO (0.1 mol dm^{-3} NEt_4ClO_4) at 25 °C[a]

	In dmf						In Me_2SO					
	Ag–AgCl (1 mol dm^{-3} NaCl)				Ferrocenium–ferrocene		Ag–AgCl (1 mol dm^{-3} NaCl)				Ferrocenium–ferrocene	
Complex	E_{pa}	E_{pc}	ΔE	$E_{\frac{1}{2}}$	$E_{\frac{1}{2}}$	$i_{pc}:i_{pa}$[b]	E_{pa}	E_{pc}	ΔE	$E_{\frac{1}{2}}$	$E_{\frac{1}{2}}$	$i_{pc}:i_{pa}$[b]
[Ni(salen)]	0.92	0.81	0.11	0.87	0.39	0.98	0.84	0.72	0.12	0.78	0.30	1.00
[Ni(salpd)]	0.85	*c*					0.73	*c*				
[Ni(saltmen)]	1.02	0.87	0.15	0.94	0.47	0.93	0.93	0.82	0.11	0.87	0.39	0.95
[Ni(α,α′-Me_2salen)]	0.88	0.77	0.12	0.82	0.35	0.99	0.80[d]	0.69[d]	0.11[d]	0.74[d]	0.26[d]	1.00[d]
[Ni(saloph)]	1.01	0.88	0.13	0.95	0.48	0.96	0.91	0.75	0.17	0.83	0.35	0.98
[Ni(salophCl$_2$)]	1.03	0.91	0.12	0.97	0.50	0.90	0.97	0.79	0.19	0.88	0.40	0.91
[Ni(3,5-Cl_2saloph)][e]	1.02	0.86	0.16	0.94	0.44	1.10	0.94	0.83	0.11	0.88	0.40	0.98

[a] All potentials in V. Solute concentration ≈ 10^{-3} mol dm^{-3}; scan rate = 0.05 V s^{-1}; E_{pa} and E_{pc} are the anodic and the cathodic peak potentials, respectively; $\Delta E = E_{pa} - E_{pc}$; $E_{\frac{1}{2}} = \frac{1}{2}(E_{pa} + E_{pc})$. [b] The ratio $i_{pc}:i_{pa}$ in dmf decreases for scan rates lower than 0.04 V s^{-1}, while in Me_2SO this behaviour is observed only for scan rates lower than 0.01 V s^{-1}. [c] Cyclic volammograms do not show the corresponding cathodic wave. [d] From ref. 11. [e] From ref. 10.

prepared in this work must have analogous structures, thus providing a rationale for the assignment of spectral bands. The very intense bands at low wavelengths have been assigned to charge-transfer transitions;[32,33] for complexes with aromatic bridges these bands occur at longer wavelengths, as expected from the higher aromaticity of the ligands which eases delocalisation of electron density.

The weaker band in the region 530–600 nm in the spectra of complexes with aliphatic imines is assigned to unresolved transitions from the four low-lying d orbitals to the empty d_{xy} orbital.[32,33] This band could not be observed for complexes with aromatic imine bridges since it is masked by the high-intensity charge-transfer transitions.

The energy of the band assigned to d–d transitions can provide a rough estimate of the ligand-field strength, since one of the electronic transitions comprised in the band envelope is $d_{xy} \longleftarrow d_{x^2-y^2}$ and the energy associated with this transition is $10Dq - C$.[33] No comparison is possible between energies for d–d transitions for complexes with aliphatic with those with aromatic imine bridges, as they are not observed in the latter complexes. However, for those with aliphatic bridges it can be inferred that an increase in the number of bridging carbon atoms is associated with a decrease in ligand field, as can be gathered from the lower energies of d–d transitions for the complex with the 1,3-propanediamine bridge; this decrease must be due to an increase in the size of the ligand cavity, as is corroborated by noting that [Ni(salpd)] has the largest Ni–N and Ni–O distances of all structures described above.

Cyclic voltammetry of nickel(II) complexes

Electrochemical data are summarised in Table 1. The compound [Ni(salpd)] is irreversibly oxidised and in foregoing discussion all references will be to the other compounds, for which in both solvents the voltammograms show one oxidation process in the potential range studied: $E_{\frac{1}{2}}$ (*vs.* Ag–AgCl) values from 0.78 to 0.97 V in dmf and from 0.63 to 0.89 V in Me_2SO. With increasing scan rates a linear dependence is observed between i_p and $v^{\frac{1}{2}}$ and between E_p and i_p. In both solvents, the anodic–cathodic peak potential separations [ΔE(dmf) = 0.11–0.16 and ΔE(Me_2SO) = 0.11–0.19 V] are similar to or somewhat larger than those observed for the ferrocenium–ferrocene couple (0.10 V in dmf and 0.09 V in Me_2SO), for which a diffusion-controlled one-electron reversible process is expected to occur under the experimental conditions used. The ratio $i_{pc}:i_{pa}$ is solvent dependent: it is practically constant and equal to 1:1 in Me_2SO (except for the scan rate of 0.01 V s^{-1}), whereas in dmf it depends on the scan rate and reaches values near 1:1 only for scan rates higher than 0.04 V s^{-1}.

In both solvents the complexes are oxidised to nickel(III) (see below); but whereas in Me_2SO the oxidation process closely resembles reversible charge transfer and the results also provide support for chemical reversibility within the cyclic voltammetric timescale used, in dmf neither chemical nor electrochemical reversibility can easily be supported, as $i_{pc}:i_{pa}$ approaches 1:1 only for scan rates higher than 0.04 V s^{-1}.[34]

Dependence of redox potentials on the ligand. The oxidation potentials are markedly dependent on the imine bridge, with the more positive potentials observed for complexes with aromatic bridges. Two possible explanations can be invoked to explain this behaviour:[4–7] (i) an increase in unsaturation that would ease electron-density delocalisation from the metal to the ligand, and (ii) higher rigidity of the ligand, imparted by the aromatic bridge, that would hinder a contraction of the hole cavity.

Substituents on the ligands affect the oxidation potentials in the usual manner:[4–12] electron-withdrawing substituents (Cl atoms) shift the redox potential positively, whereas electron-donating groups (methyls on the imine carbon) have the opposite effect. Nevertheless, the above arguments cannot account for the observed effect of the methyl group on the $E_{\frac{1}{2}}$ of [Ni(saltmen)] as the introduction of these methyl groups, despite having a positive inductive effect, produces an anodic shift in the redox potential relative to that of [Ni(salen)]. Based on the X-ray data obtained for the similar complex [Ni(naptmen)] [H_2naptmen = *N*,*N*′-bis(2-hydroxynaphthylmethylene)-2,3-dimethylbutane-2,3-diamine], this observation is consistent with the interpretation that steric hindrance on axial binding sites, imposed by the axially oriented methyl groups of the imine bridge, decreases stabilisation of Ni^{III} by co-ordinated solvent molecules.[11,35]

Dependence of redox potentials on the solvent. The redox potentials show a cathodic shift with an increase in the donor capacity of the solvent. Oxidation of square-planar nickel(II) complexes to Ni^{III} takes place with a concomitant increase in co-ordination number, as these latter complexes are normally six-co-ordinate. The cathodic shift in the redox potentials on going from dmf to Me_2SO is attributed to the stronger axial bonds that are established between nickel(III) and the molecules of the better donor, and that help to stabilise the high oxidation state of the metal (see below).

Electrolysis of nickel(II) complexes and EPR spectra of the oxidised species

Electrochemical oxidation in these solvents produces a change from reddish to dark brown, implying formation of new species. The observation that EPR spectra of fluid solutions of the electrolysed complexes exhibit a single broad line, with g_{iso} in the range 2.197–2.210 for dmf and 2.161–2.192 in Me_2SO, implies a metal-centred oxidation process, which for nickel must be

Table 2 The EPR parameters for $[NiL(dmf)_2]^+$ and $[NiL(Me_2SO)_2]^+$ complexes

	Experimental values					Coefficients[a]			Energy of excited states/cm^{-1}		
Complex	g_x	g_y	g_z	g_{av}[b]	g_{iso}[c]	C_1	C_2	C_3	$\Delta(^2B_1)$	$\Delta(^2A_2)$	ΔQ[d]
$[Ni(salen)(dmf)_2]^+$	2.266	2.222	2.021	2.170	2.199	0.0343	0.0424	0.1075	11 465	9275	3658
$[Ni(salen)(Me_2SO)_2]^+$	2.256	2.216	2.020	2.164	2.183	0.0334	0.0399	0.1045	11 774	9856	3763
$[Ni(saltmen)(dmf)_2]^+$	2.265	2.224	2.020	2.170	2.210	0.0348	0.0414	0.1053	11 300	9499	3734
$[Ni(saltmen)(Me_2SO)_2]^+$	2.254	2.226	2.020	2.167	2.186	0.0351	0.0396	0.1047	11 204	9931	3756
$[Ni(\alpha,\alpha'\text{-}Me_2salen)(dmf)_2]^+$	2.274	2.220	2.018	2.171	2.198	0.0346	0.0432	0.1010	11 366	9103	3894
$[Ni(\alpha,\alpha'\text{-}Me_2salen)(Me_2SO)_2]^+$[e]	2.266	2.220	2.021	2.169	2.188	0.0340	0.0414	0.1074	11 566	9499	3662
$[Ni(saloph)(dmf)_2]^+$	2.259	2.218	2.022	2.166	*f*	0.0334	0.0400	0.1092	10 704	8938	3274
$[Ni(saloph)(Me_2SO)_2]^+$	2.252	2.214	2.021	2.162	2.182	0.0329	0.3900	0.1065	10 866	9167	3357
$[Ni(salophCl_2)(dmf)_2]^+$	2.254	2.216	2.022	2.164	*f*	0.0331	0.0392	0.1089	10 801	9120	3283
$[Ni(salophCl_2)(Me_2SO)_2]^+$	2.251	2.214	2.021	2.162	2.161	0.0329	0.0389	0.1064	10 866	9190	3360
$[Ni(3,5\text{-}Cl_2saloph)(dmf)_2]^+$[g]	2.238	2.204	2.023	2.155	*f*	0.0308	0.0363	0.1099	11 607	9848	3253
$[Ni(3,5\text{-}Cl_2saloph)(Me_2SO)_2]^+$[g]	2.234	2.204	2.020	2.153	2.168	0.0313	0.0361	0.1029	11 422	9903	2474

[a] Obtained from McGarvey equations, see text. [b] The value of g_{av} was calculated as $\frac{1}{3}(g_x + g_y + g_z)$. [c] Obtained from fluid-solution EPR spectra at 233 K. [d] Difference between the average energy of the quartet states and the ground state. [e] From ref. 11. [f] It was not possible to obtain fluid-solution EPR spectra, see text. [g] From ref. 10.

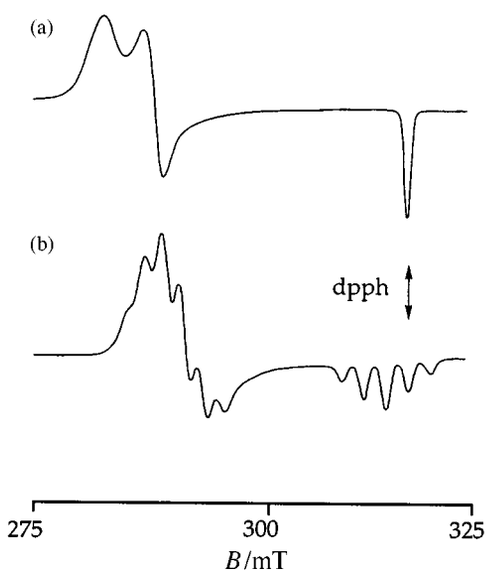

Fig. 1 Frozen-solution X-band EPR spectra at −140 °C of (a) an electrochemically oxidised solution of [Ni(salen)] in dmf and (b) the corresponding pyridine adduct

associated with the +3 formal oxidation state. Oxidised complex solutions decay, at room temperature, to EPR-silent solutions; the decomposition rates are dependent on the ligand,[13] but are always faster in dmf (half-lives of 10 min) than in Me_2SO (up to 2 h). The decay in dmf is significantly slower at −20 °C (half-lives similar to those in dimethyl sulfoxide), and the samples are stable in both solvents for several days when kept frozen in liquid nitrogen. The half-lives in dmf are in accordance with the chemical irreversibility associated with the charge-transfer process in cyclic voltammetry.

The time elapsed during electrolysis in either solvent was typically 20 min corresponding roughly to the moment where formation of the oxidised species becomes slower than their decomposition, as can be inferred by following the variation of the intensity of the derivative EPR bands with electrolysis time. The concentrations of the nickel(III) compounds at the end of the electrolysis, under the conditions used, were estimated by EPR spectroscopy to be *ca.* 30 to 50% of the total nickel in solution.

Frozen-solution EPR spectra of the electrolytically generated nickel complexes show rhombic symmetry, large *g* tensor anisotropy and are typical of nickel(III) complexes in low-spin ($S = \frac{1}{2}$) electron configuration.[1,4–12,36–39] No hyperfine splittings could be detected in any of the three *g* regions [Fig. 1(a)].

In the absence of EPR crystal data for the nickel(III) complexes studied, the observed similarity between their *g* features and those of analogous cobalt(II) compounds[40] can be extended to support the following orientation scheme for the tensor axes of the nickel complexes: $g_1 = g_x$, $g_2 = g_y$, $g_3 = g_z$, where g_1 and g_3 refer to the lowest and highest magnetic field *g* values, respectively. The EPR data for the nickel(III) species in dmf and in Me_2SO are summarised in Table 2.

Pyridine adducts

Addition of pyridine to freshly prepared solutions of the nickel(III) complexes in Me_2SO, at room temperature, and in dmf, at temperatures just above the softening point of the frozen glass, gave new species in solution as can be inferred from the rapid change to yellow-red in the first solvent and to yellow-brown in the latter solvent.

Frozen solution of pyridine adducts in Me_2SO are EPR silent, but the pyridine adducts in dmf exhibit frozen-solution EPR spectra of rhombic type, with large *g* tensor anisotropy and g_{av} in the range 2.12–2.14, and show hyperfine couplings in all *g* regions. The observation of one well resolved quintuplet ($a = 2.14$–2.27 mT) in the region of higher magnetic field, and two non-resolved quintuplets in the two other *g* regions, imply the existence in dmf of six-co-ordinate nickel(III) species with two pyridines axially bound [Fig. 1(b)]. The similarity between *g* patterns of these species with those obtained in dmf and Me_2SO in the absence of pyridine supports the same orientation scheme for the tensor axes of the pyridine adducts. The EPR parameters for $[NiL(py)_2]^+$ are summarised in Tables 3 and 4.

No EPR signals could be detected in fluid solutions of dmf, even at temperatures just above the freezing point. This result combined with the observation that pyridine adducts in Me_2SO are also EPR silent indicates that nickel(III) pyridine adducts have very short lifetimes in fluid solutions. No extensive characterisation of the pyridine adducts in Me_2SO and in fluid dmf solutions was pursued, but their solution electronic spectra indicate only the presence of nickel(II) species, thus suggesting that under these experimental conditions very fast decomposition of the nickel(III) species occurs.

Electronic spectra of nickel(III) species

Electronic spectral data for nickel(III) species in Me_2SO are included in Table 5; there are no data for dmf solutions as decomposition of the nickel(III) species is faster in this solvent and only very low-intensity spectra could be observed. However, for $[Ni^{III}(salen)]^+$ the decomposition rate in dmf is slow enough to allow the observation of its spectrum, and the

Table 3 The EPR parameters for $[NiL(py)_2]^+$ complexes

	Experimental g values				Coefficients			Energy of excited states/cm^{-1}		
Ligand (L)	g_x	g_y	g_z	g_{av} [a]	C_1	C_2	C_3	$\Delta(^2B_1)$	$\Delta(^2A_2)$	ΔQ
salen	2.201	2.172	2.024	2.132	0.025	0.030	0.109	15 667	13 196	3588
saltmen	2.214	2.186	2.022	2.141	0.028	0.032	0.106	14 146	12 137	3710
α,α′-Me_2salen	2.201	2.175	2.027	2.134	0.025	0.029	0.116	15 667	13 422	3387
saloph	2.190	2.164	2.024	2.126	0.024	0.028	0.109	15 084	12 814	3280
salophCl$_2$	2.189	2.162	2.022	2.124	0.024	0.028	0.104	15 084	12 722	3428
3,5-Cl_2saloph [b]	2.180	2.160	2.025	2.122	0.023	0.003	0.111	15 610	13 700	3240

[a] The adducts are not stable in fluid solutions; no experimental values for g_{iso} could be obtained; g_{av} were used, with $\langle g_{av} \rangle = \frac{1}{3}(g_x + g_y + g_z)$. [b] From ref. 10.

Table 4 Nitrogen-14 superhyperfine coupling constants and spin densities for $[NiL(py)_2]^+$ complexes

	Experimental superhyperfine coupling [a]				Anisotropic superhyperfine tensor		Spin densities on ^{14}N			
Base	A_x	A_y	A_z	A_{av} [b]	$A_{xx,yy}$	A_{zz}	C_{2s}^2	C_{2p}^2	total [c] (%)	λ^2
salen	1.65	1.76	2.14	1.85	−0.15	0.28	0.033	0.084	23.4	2.5
saltmen	1.82	1.63	2.14	1.86	−0.14	0.27	0.033	0.080	22.7	2.4
α,α′-Me_2salen	1.66	1.68	2.14	1.83	−0.16	0.30	0.033	0.091	24.7	2.8
saloph	1.60	1.60	2.22	1.81	−0.20	0.40	0.032	0.119	30.4	3.7
salophCl$_2$	1.60	1.60	2.27	1.83	−0.22	0.44	0.033	0.130	32.6	4.0
3,5-Cl_2saloph [b]	1.62	1.78	2.25	1.88	−0.18	0.36	0.034	0.107	28.2	3.2

[a] The A values are expressed in mT. [b] The A_{iso} could not be obtained for the adducts and A_{av} values are used instead, with $\langle A_{av} \rangle = \frac{1}{3}(A_x + A_y + A_z)$. [c] Spin density delocalised onto the two axial nitrogen atoms. [d] From ref. 10.

Table 5 Electronic spectral data for $[NiL(Me_2SO)_2]^+$ complexes

Complex	Experimental values [a]	Calculated values [b]	ξ [c]
$[Ni(salen)(Me_2SO)_2]^+$	940 (br) (600), 640 (sh) (490)	850, 980, 640	393
$[Ni(saltmen)(Me_2SO)_2]^+$	970 (br) (670), 650 (sh) (530)	910, 980, 650	393
$[Ni(\alpha,\alpha'\text{-}Me_2saltmen)(Me_2SO)_2]^+$	915 (br) (690), 730 (sh) (520)	880, 1040, 730	393
$[Ni(saloph)(Me_2SO)_2]^+$	1020 (br) (500), *d*	960, 1100, *d*	357
$[Ni(salophCl_2)(Me_2SO)_2]^+$	1000 (br) (770), *d*	950, 1050, *d*	357
$[Ni(3,5\text{-}Cl_2saloph)(Me_2SO)_2]^+$ [e]	1070 (br) (500), 660 (sh) (400)	980, 1150, 660	357

[a] Band maxima expressed in nm; molar absorption coefficients, in parentheses, expressed in $dm^3\ mol^{-1}\ cm^{-1}$; br = broad, sh = shoulder. [b] Obtained by deconvolution of the experimental absorption spectra. [c] Calculated to get the best fit between the transition energies obtained from electronic spectra and calculated from EPR parameters. [d] Obscured by high-intensity charge-transfer bands. [e] From ref. 10.

similarity between the spectra recorded in both solvents was taken to presuppose that the spectra of the other complexes should be analogous in both solvents.

Room-temperature electronic spectra of the oxidised solutions show a very broad band in the near-IR region, $880 < \lambda_{max} < 1040$ nm, with molar absorption coefficients in the range 600 to 900 $dm^3\ mol^{-1}\ cm^{-1}$. For some complexes a higher-energy band ($640 < \lambda_{max} < 750$ nm, $\varepsilon = 490$–$820\ dm^3\ mol^{-1}\ cm^{-1}$) only discernible as a shoulder on a very intense charge-transfer band ($\varepsilon = 5000\ dm^3\ mol^{-1}\ cm^{-1}$) could also be observed. Owing to decomposition of nickel(III) species in fluid solution these bands disappear, and in a few hours the spectra revert to those of planar diamagnetic nickel(II) species.

No electronic spectra for $[NiL(py)_2]^+$ could be obtained under the experimental conditions used, since their respective lifetimes in fluid solution were not long enough to allow the recording.

Electronic structure of the nickel(III) species

We assume that, similarly to the nickel(II) precursor complexes, nickel(III) pyridine adducts have a $C_{2v}(x)$ molecular symmetry [33,40] with an almost planar equatorial N_2O_2 environment. As $g_z < g_x$, g_y and the larger nitrogen hyperfine splittings are observed in the g_z component, the unpaired electron must lie in an orbital which is predominantly d_{z^2}, implying a $^2A_1$ ground state for these species [7–12,36–39,41] ($^2A_1 = a\ d_{z^2} + b\ d_{x^2-y^2}$; assuming a mixture of d_{z^2} and $d_{x^2-y^2}$ allowed in this symmetry, and with $a \gg b$ [41]).

This ground state is observed in the majority of known six-co-ordinate nickel(III) complexes [7–12,36–39] and the same ground state is assumed for nickel(III) complexes in pure solutions of dmf and Me_2SO, since the pattern of g values is very similar to those of $[NiL(py)_2]^+$; the nickel(III) complexes in pure solutions are thus formulated as $[NiL(solv)_2]^+$ (solv = dmf or Me_2SO).

None of the nickel(III) species exhibits EPR spectra for which hyperfine splittings due to in-plane nitrogen ligand atoms could be observed. This result has correspondence in analogous cobalt(II) complexes with $^2A_1(d_{z^2})^1$ electronic configuration, [40,41] and in axially elongated six-co-ordinate nickel(III) complexes with N-bound equatorial ligands. [36–39] This behaviour has been interpreted as to imply that delocalisation of unpaired spin density to the equatorial ligand takes place mainly through the ligand system. We assume that a similar explanation will hold for our complexes, corroborating the previous assumption of a ground state that is essentially d_{z^2} in character.

The electronic spectra of oxidised solutions of the complexes are similar to those reported for other six-co-ordinate low-spin nickel(III) complexes with $^2A_1(d_{z^2})^1$ ground state. [7–10,36–38,42] Band assignment was made assuming: (i) the high-intensity bands in the visible region are due to allowed charge-transfer transitions from ligand to Ni^{III} [superimposed on charge-transfer bands to nickel(II), as the electrolysis were not complete; see above] and (ii) that the two medium-intensity bands in the near-infrared region can be assigned to nickel(III) d–d transitions, since the

spectra of precursor nickel(II) complexes do not show any band at wavelengths longer than 600 nm.

To assign d–d bands, we made use of the d-orbital ordering $d_{xy} > d_{z^2} > d_{xz}, d_{yz} > d_{x^2-y^2}$, as proposed by Hitchman[43] for the homologous cobalt(II) complexes and which has been applied to spectrum of the similar complex [Ni(3,5-Cl_2saloph)]$^+$.[10] Deconvolution of the broad band yielded two bands at slightly different energies (Table 5) which are assigned to the electronic transitions $d_{xz} \longleftarrow d_{z^2}$ ($^2B_1 \longleftarrow {}^2A_1$) and $d_{yz} \longleftarrow d_{z^2}$ ($^2A_2 \longleftarrow {}^2A_1$). The shoulder in the visible region must correspond to the $d_{xy} \longleftarrow d_{z^2}$ ($^2B_2 \longleftarrow {}^2A_1$) transition.

Additional information on the electronic structure of nickel(III) species can be gathered from analysis of the EPR parameters using the model developed by McGarvey[41] for d^7 systems. Application of this model to a $^2A_1(d_{z^2})$ ground state, in conjunction with the approximation suggested by Labause and Raynor[44] which uses a single (average) value for the energy of the quartet states, allows for the derivation of equations (1a)–(1c) for the g tensor[10] where $C_1 = \xi/\Delta(^2B_1)$, $C_2 = \xi/\Delta(^2A_2)$ and

$$g_z = 2.0023 + 2C_3^2 + 3C_1C_2 - 3C_2^2 - 2C_1^2 \quad (1a)$$

$$g_x = 2.0023 + 2C_3^2 - 3C_1C_2 - 3C_1^2 + 6C_2 \quad (1b)$$

$$g_y = 2.0023 + 2C_3^2 - 3C_1C_2 - 3C_2^2 + 6C_1 \quad (1c)$$

$C_3 = \xi/\Delta(^4B_2)$; $\Delta(^n\Gamma_i)$ is the energy difference between the $^n\Gamma_i$ excited state and the ground state ($^2A_1$), and ξ is the one-electron spin–orbit coupling constant. The values of C_1 and C_2 yield approximate values for the energies of the excited states $^2B_1$ and $^2A_2$ relative to the ground state $^2A_1$.

The reduction of the spin–orbit coupling constant was estimated by finding the value of ξ which minimises the difference between the values of $\Delta(^2B_1)$ and $E(^2A_1)$ obtained by EPR spectra analysis and that obtained from the electronic spectra. In Me_2SO the values so obtained indicate a reduction of the spin–orbit coupling constant of 50% for complexes with saloph and salophCl$_2$, and a value of 55% for the other complexes (Table 5), values that are in good agreement with those for [Ni(3,5-Cl_2saloph)][10] and several other six-co-ordinate nickel(III) complexes.[7,36–39] Furthermore, the spin–orbit coupling constant for the complexes and the C_3 values enable an estimate of the (average) energy of low-lying excited quartet states (ΔQ).

For complexes with axially bound dmf and pyridine it was not possible to estimate spin–orbit coupling constants using the procedure described above, as their electronic spectra could not be recorded, and the energy of the excited states was calculated using the same spin–orbit coupling constants as in Me_2SO.

In Tables 2 and 3 are included the calculated values of $\Delta(^2B_1)$, $\Delta(^2A_2)$ and ΔQ for $[NiL(dmf)_2]^+$, $[NiL(Me_2SO)_2]^+$ and $[NiL(py)_2]^+$. The importance of quartet states to the spin-Hamiltonian parameters must be stressed, as their calculated (average) values are non-negligible, typically in the range of 2880–3990 cm^{-1} above the ground state.

Energy of excited states

No detailed theoretical analysis has been presented, so far, to explain the factors that affect the electronic structure of six-co-ordinate low-spin nickel(III) complexes, but a detailed analysis for isoelectronic cobalt(II) salen-type complexes has been provided by Hitchman.[43] The calculations showed that an increase in axial field and/or a raising of the cobalt atom from the co-ordination plane increases markedly the energy of the excited doublets, but only induces a small lowering of the energy of the quartet states. However, the latter energy does show a significant dependence on the in-plane ligand field: the greater its strength, the higher is the energy of the quartet state. Analysis of the data in Table 2 and 3 shows that the energy of the doublet and quartet states of nickel(III) complexes comply to Hitchman predictions for cobalt(II).

Effect of the axial co-ordination. First, it must be pointed out that no significant dependence of the energy of excited quartets on the strength of axial ligation was observed. On the other hand, an increase in donor strength of the axial ligand (characterised by donor number:[45] dmf < Me_2SO < pyridine) is accompanied by an increase in the energy of the excited doublets, due to stronger interaction of the axial ligands with the d_{z^2} orbital. The observed decrease in g_x and g_y when the axially bound molecules change from dmf to Me_2SO and to pyridine can thus be accounted for by recalling that an increase in the energy of the excited doublets will make C_1 and C_2 smaller. In fact, neglecting second-order terms, equations (1) can be expressed as $g_x = 2.0023 + 6C_2$ and $g_y = 2.0023 + 6C_1$, and a raising in the energy of d_{z^2} relative to d_{yz} and d_{xz} would decrease C_2 and C_1 and thus g_x and g_y.

Effect of the equatorial ligand. Data in Tables 2 and 3 reveal that the average energies of the quartet states are more dependent on the equatorial ligand than those of the doublets and, for each axial ligand, complexes with aliphatic bridges have energies higher than those with aromatic bridges. Furthermore, as the energy of the quartet states is directly related to the in-plane ligand field, it is possible to infer that equatorial ligand fields are weaker in complexes with aromatic bridges.

Partially to circumvent the lack of structural data needed to correlate the strength of equatorial ligands with distances from the nickel(III) centres to the co-ordinated atoms, some structural details of the corresponding nickel(II) complexes will be used. In complexes with aromatic bridges the Ni–N bond distances are longer than the Ni–O bonds, a situation to be contrasted with those with aliphatic bridges for which the Ni–N bond distances are shorter. This behaviour is attributed to the stiffness of the aromatic bridge which imposes a bite size which the metal ion has to accommodate, absent in those with aliphatic bridges, which have the possibility to adapt its conformation to provide a better fit to the metal-ion size.[4–7] On oxidation, as the ionic radius of nickel ion decreases it is to be expected that those ligands with stiff and large bite will be less prone to adjust the hole cavity to the size of the metal ion, consequently ligands with aromatic bridges will impose weaker ligand fields in nickel(III) complexes.

Nitrogen hyperfine tensor and spin density on nitrogen atoms of axial bound pyridines

For the nitrogen atoms of the axial base the 2s spin densities (C_{2s}^2) are obtained from the isotropic nitrogen coupling constants ($C_{2s}^2 = A_{iso}/A_s^{100}$; $A_s^{100} = 55.7$ mT),[46] whereas the principal value of the anisotropic tensor (A_{zz}) gives the 2p spin densities ($C_{2p}^2 = A_{zz}^{corr}/A_p^{100}$; $A_s^{100} = 3.35$ mT).[46] As the unpaired electron in the d_{z^2} nickel orbital interacts directly with the pyridine nitrogen atoms, the signs of the experimental isotropic hyperfine tensor components and those of experimental values of A_z(N), A_x(N) and A_y(N) are taken to be positive.[46] The anisotropic hyperfine tensor was calculated after correction for indirect dipolar coupling using the point–dipole approximation[46] and a value of 200 pm for the Ni–N axial bond distance, as observed in other nickel(III) complexes for which the molecular structure has been determined.[47]

The 2s and 2p spin densities, the ratio p : s ($\lambda^2 = C_{2p}^2/C_{2s}^2$) and the total spin density delocalised onto the axially bounded pyridine are reported in Table 4. The values of C_{2s}^2 are practically insensitive to changes in the equatorial ligand ($0.032 < C_{2s}^2 < 0.035$), whereas those of C_{2p}^2 show larger variations ($0.080 < C_{2p}^2 < 0.130$); thus changes in λ^2 reflect primarily changes in this latter quantity.

When the complexes are grouped by their λ^2 values, those with aromatic bridges show the highest values. As λ^2 reflects primarily the 2p spin densities on the nitrogen atoms, the larger p character of the nitrogen lone pair directed to the metal will

imply longer (weaker) axial bonds for complexes with aromatic bridges, a result that agrees with the observation that these nickel(III) complexes exhibit the lowest values for doublet states.

The total spin density delocalised onto the axial N atoms is also greater in complexes with aromatic bridges, an observation that can be interpreted as to imply that the more extensive delocalised equatorial ligands will act as stronger π donors to nickel(III).

Conclusion

The oxidation of nickel(II) complexes in the strong donating solvents dmf and Me_2SO was shown to proceed through oxidation of the metal centre, giving nickel(III) species to which solvent molecules are axially co-ordinated. The importance of strong axial co-ordination in the stabilisation of the +3 oxidation state became apparent from the potential cathodic shift observed as the donating ability of the axially co-ordinated molecules increases, and by the observation that [Ni(saltmen)], which exhibits axial steric hindrance, shows one of the more positive oxidation potentials.

In each solvent, shifts in oxidation potentials can be rationalised by arguments that are in a broad sense similar to those put forward for macrocyclic nickel complexes. Moreover, structural flexibility in the diimine bridge was found to play a key role in controlling the oxidation potentials: ligands with aliphatic imine bridges allow a more facile closing of the hole cavity best to accommodate changes in size on going from Ni^{II} to Ni^{III}, and thus show less positive potentials when compared to those with aromatic bridges, as the latter's rigidity makes them less prone to adjust to the decrease in metal size upon oxidation.

Electronic characterisation of nickel(III) complexes has shown that the energy of the low-lying excited doublets is more dependent on the axially co-ordinated ligand, whereas the energy of the excited quartets shows greater dependence on the equatorial ligand. This latter relationship allowed us to propose that ligands with aromatic imine bridges have in-plane ligand fields that are weaker than those with aliphatic bridges.

The final point to be considered here concerns the effect of the axially co-ordinated ligands on the lifetime of the nickel(III) species: the faster rates of decomposition of the complexes were observed for the weaker (dmf) and the stronger (pyridine) donors. However, the reduced set of axial ligands used prevented us proposing any mechanism for the decomposition of Ni^{III}.

We are extending these studies to other nickel(III) complexes by selecting two main approaches: (i) to increase ligand aromaticity in the aldehyde moiety, to get further insights into the effect of unsaturation on ligand-field strength, and (ii) to use a large number of N-donor Lewis bases as axial ligands to probe the decomposition paths of the nickel(III) complexes.

Acknowledgements

This work was partially supported by the Fundação para a Ciência e Tecnologia (Lisboa) through project Praxis/2/2.1/QUI/316/94.

References

1 (*a*) A. F. Kolodziej, *Prog. Inorg. Chem.*, 1994, **41**, 493; (*b*) R. Cammack, *Adv. Inorg. Chem.*, 1988, **32**, 297; (*c*) *Bioinorganic Chemistry of Nickel*, ed. J. R. Lancaster, jun., VCH, New York, 1988.
2 H. Yoon, T. R. Wagler, K. O'Connor and C. J. Burrows, *J. Am. Chem. Soc.*, 1990, **112**, 4568 and refs. therein.
3 D. P. Mack and P. B. Dervan, *J. Am. Chem. Soc.*, 1990, **112**, 4604.
4 D. H. Busch, *Acc. Chem. Res*, 1978, **11**, 392; (*b*) F. V. Lovecchio, E. S. Gore and D. H. Busch, *J. Am. Chem. Soc.*, 1974, **96**, 3109; J. A. Streeky, D. G. Pillsbury and D. H. Busch, *Inorg. Chem.*, 1980, **19**, 3148.
5 K. M. Kadish, *Prog. Inorg. Chem.*, 1986, **34**, 435.
6 A. M. Stolzenberg and M. T. Sterishic, *Inorg. Chem.*, 1988, **27**, 1614.
7 A. Buttafava, L. Fabbrizi, A. Perotti, A. Poggi, G. Poli and B. Seghi, *Inorg. Chem.*, 1986, **25**, 1456; A. Bencini, L. Fabbrizi and A. Poggi, *Inorg. Chem.*, 1981, **20**, 2544.
8 H.-J. Krüger and R. H. Holm, *Inorg. Chem.*, 1989, **28**, 1148; H.-J. Krüger, G. Peng and R. H. Holm, *Inorg. Chem.*, 1991, **30**, 734.
9 F. P. Bossu and D. W. Margerum, *Inorg. Chem.*, 1977, **16**, 1210.
10 B. de Castro and C. Freire, *Inorg. Chem.*, 1990, **29**, 5113.
11 M. A. A. de C. T. Carrondo, B. de Castro, A. M. Coelho, D. Domingues, C. Freire and J. Morais, *Inorg. Chim. Acta*, 1993, **205**, 157.
12 F. Azevedo, M. A. A. de C. T. Carrondo, B. de Castro, M. Convery, D. Domingues, C. Freire, M. T. Duarte, K. Nielson and I. Santos, *Inorg. Chim. Acta*, 1994, **219**, 43.
13 B. de Castro, C. Freire and E. Pereira, *J. Chem. Soc.*, *Dalton Trans.*, 1994, 571.
14 E. Pereira, L. Gomes and B. de Castro, *Inorg. Chim. Acta*, 1998, **271**, 83.
15 E. Pereira, L. Gomes and B. de Castro, *J. Chem. Soc.*, *Dalton Trans.*, 1998, 629.
16 R. H. Holm, G. W. Everett, jun. and A. Chakravorty, *Inorg. Chem.*, 1966, **7**, 183.
17 C. Gosden, J. B. Kerr, D. Pletcher and R. Rosas, *J. Electroanal. Chem.*, *Interfacial Electrochem.*, 1981, **117**, 101; A. A. Isse, A. Gennno and E. Vianello, *Electrochim. Acta*, 1992, **37**, 113.
18 A. Kaptorkiewicz and B. Behr, *Inorg. Chim. Acta*, 1983, **69**, 247.
19 K. A. Goldsby, *J. Coord. Chem.*, 1988, **19**, 83; K. A. Goldsby, J. K. Blaho and L. A. Hoferkamp, *Polyhedron*, 1989, **8**, 113; K. A. Goldsby and L. A. Hoferkamp, *Chem. Mater.*, 1989, **1**, 348.
20 P. Audebert, P. Capdevielle and M. Maumy, *New J. Chem.*, 1991, **15**, 235; *Synth. Met.*, 1991, **41**, 3049; *New J. Chem.*, 1992, **16**, 697.
21 C. E. Dahm and D. G. Peters, *J. Electroanal. Chem.*, *Interfacial Electrochem.*, 1996, **406**, 119; **410**, 163.
22 M. Vilas-Boas, C. Freire, B. de Castro, P. A. Christensen and A. R. Hillman, *Inorg. Chem.*, 1997, **36**, 4919.
23 R. Sayre, *J. Am. Chem. Soc.*, 1955, **77**, 6689.
24 S. T. Donald, jun., *Experimental Electrochemistry for Chemistry*, Wiley, New York, 1974.
25 D. Chen and A. E. Martell, *Inorg. Chem.*, 1987, **26**, 1026.
26 J. R. Pilbrow and M. E. Winfield, *Mol. Phys.*, 1973, **25**, 1073.
27 C. P. Pool, jun., *Electron Spin Resonance*, Wiley, New York, 2nd edn., 1983.
28 A. G. Manfredotti and C. Guastini, *Acta Crystallogr.*, *Sect. C*, 1983, **39**, 863.
29 M. G. B. Drew, R. N. Prasad and R. P. Sharma, *Acta Crystallogr.*, *Sect. C*, 1985, **41**, 1755.
30 A. Radha, M. Seshasayee, K. Ramalingam and G. Aravamudan, *Acta Crystallogr.*, *Sect. C*, 1985, **41**, 1169.
31 F. Akhtar, *Acta Crystallogr.*, *Sect. B*, 1981, **37**, 84.
32 A. B. P. Lever, *Inorganic Electronic Spectroscopy*, Elsevier, New York, 2nd edn., 1984.
33 G. Maki, *J. Chem. Phys.*, 1958, **28**, 651.
34 A. J. Bard and L. R. Faulkner, *Electrochemical Methods*, Wiley, New York, 1980.
35 D. F. Averill and R. F. Broman, *Inorg. Chem.*, 1978, **17**, 3389.
36 E. S. Gore and D. H. Busch, *Inorg. Chem.*, 1973, **12**, 1.
37 J. M. Bemtgen, H. R. Gimpert and A. von Zelewsky, *Inorg. Chem.*, 1983, **22**, 3576.
38 A. Desideri, J. B. Raynor and C. K. Poon, *J. Chem. Soc.*, *Dalton Trans.*, 1977, 2051.
39 L. F. Mehne and B. B. Wayland, *Inorg. Chem.*, 1975, **14**, 881.
40 C. Daul, C. W. Schlapfer and A. von Zelewsky, *Struct. Bonding* (*Berlin*), 1970, **36**, 129.
41 B. R. McGarvey, *Can. J. Chem.*, 1975, **53**, 2498.
42 G. V. R. Chandramouli and P. T. Manoharan, *Inorg. Chem.*, 1987, **26**, 3291.
43 M. A. Hitchman, *Inorg. Chem.*, 1977, **16**, 1985; *Inorg. Chim. Acta*, 1977, **26**, 237.
44 G. Labause and J. B. Raynor, *J. Chem. Soc.*, *Dalton Trans.*, 1980, 2388; 1981, 590.
45 V. Gutman, *The Donor–Acceptor Approach to Molecular Interaction*, Plenum, New York, 1978.
46 B. A. Goodman and J. B. Raynor, *Adv. Inorg. Chem. Radiochem.*, 1970, **13**, 135.
47 M. Yamashita, K. Toriumi and T. Ito, *Acta Crystallogr.*, *Sect. C*, 1985, **41**, 1607; K. Wieghardt, W. Walz, B. Nuber, J. Weiss, A. Ozarowski and H. Stratmeier, *Inorg. Chem.*, 1986, **25**, 1650.

Received 17*th November* 1997; *Paper* 7/08231B